IEEE Transactions on Nuclear Science, Vol. NS-30, No. 4, August 1983

STUDIES OF THE HELIX CONTROLLED BEAM FRONT ACCELERATOR CONCEPT*

W. W. Destler, P. G. O'Shea, M. Reiser, C. D. Striffler, D. Welsh, and H. H. Fleischmann†

Electrical Engineering and Physics Departments
University of Maryland
College Park, Maryland 20742

†On leave from Cornell University, Ithaca, New York, 14850

Summary

Helix controlled collective ion acceleration involves the use of a helical slow wave structure to control the propagation velocity of an intense relativistic electron beam front, in which ions could be trapped and accelerated to high energy. Experimental and theoretical studies of the propagation of an IREB inside both cylindrical and helical conducting boundary systems have been conducted. In the experiments, an IREB (1 MeV, 30 kA, 30 ns, confined by an applied axial magnetic field) is injected from a 1 cm diameter hollow stainless steel cathode through a 2.4 cm diameter hole in a stainless steel anode into either cylindrical or helical downstream drift chambers. Beam propagation in the cylindrical systems is in good qualitative agreement with theoretical calculations based on a modified Bogdankevich, Rukhadze beam model.[3] When a helical slow wave structure is used as the conducting boundary, the beam front velocity is significantly reduced to values approaching those associated with the helix pitch angle.

I. Introduction

The Helix Controlled Beam Front Accelerator[1,2] a concept first proposed by H. Kim, involves the use of a helical slow wave structure to control the propagation velocity of an intense relativistic electron beamfront. Positive ions can then be trapped in the space charge potential well at the beamfront and accelerated to high energy by varying the helix pitch angle along its length. The concept is dependent upon the fact that the maximum electron current that can propagate in a grounded cylindrical drift tube is limited to values less than or equal to the space charge limiting current, given approximately by

$$I_L = \frac{17{,}000(\gamma_o^{2/3} - 1)^{3/2}}{(1 + 2\ \ell n \frac{R_w}{R_b})(1 - f)}\ [A] \qquad (1)$$

where γ_o is the relativistic mass factor of the injected electrons, R_w is the tube radius, R_b is the beam radius, and f is the fractional neutralization, if any, provided by ions.[3] If the tube is initially charged to a negative potential V_o, the electron energy will be reduced to a value given by $\gamma = \gamma_o - eV_o/m_oc^2$, thus reducing the limiting current substantially. An electron beam with $I < I_L$ in the unbiased drift tube could be effectively prevented from propagating in the biased tube by this effect. If the input end of the biased tube were then shorted to ground, a grounding wave would propagate along the cylinder at the phase velocity of transmission line waves in such a system. For a simple cylindrical boundary system, this velocity would be c. For a helical slow wave structure of radius a inside of an outer conducting boundary of radius b, this velocity is given at low frequencies by

$$v_{ph} = \frac{c\ \sin(\psi)}{\left[1 + \left(\frac{1 - a^2/b^2}{2\ \ell n\ b/a} - 1\right)\cos^2\psi\right]^{1/2}} \qquad (2)$$

and at high frequencies by $v_{ph} = c\ \sin(\psi)$ where ψ is the helix pitch angle. In this manner, the propagation velocity of the electron beam front could be controlled by varying the helix pitch along its length.

In experiments to date, the initial charging of the helix has been accomplished by the early part of the electron beam pulse. The grounding of the input end of the helix was accomplished by surface breakdown across an insulating support. The pitch of the helix was chosen to match the ion velocity readily obtained in such systems without the helix. For a 1 MeV electron beam a helix pitch in the range 0.05-0.1 was used,[2] and an enhancement of the accelerated ion energy over that achieved without a helical slow wave structure of a factor of two was achieved. In this paper, we report a systematic study of the electron beam propagation characteristics in both cylindrical and helical conducting boundary systems as a function of applied magnetic field.

II. Experiments

The general experimental configuration is shown in Fig. 1. An intense relativistic electron beam (1 MeV, 30 kA, 30 ns FWHM) is emitted from a 1 cm diameter hollow stainless steel cathode 1.2 cm upstream of a stainless steel anode plate. A 2.4 cm diameter hole in the anode allows virtually all of the electron beam current to pass into the downstream drift tube. An axial magnetic guide field constrains the radial motion of the beam electrons over the entire experimental length. The current reaching the end of the drift tube is measured using a low impedance Faraday cup.

Beam Propagation in Cylindrical Drift Tubes. The peak electron beam current measured at the downstream end of the drift tube using the Faraday cup is plotted as a function of applied magnetic field for two different diameter drift tubes (grounded at the input end) in Fig. 2. Two important features are apparent from these results: 1) The maximum current that can be propagated is independent of tube radius , and 2) The propagated current at high magnetic fields is greater for the 3.8 cm diameter tube than for the 9.8 cm diameter tube. Both of these results are in qualitative agreement with theoretical expectations.

Beam Propagation in Helical Slow Wave Structures. The peak propagated current measured at the downstream end of two different 3.8 cm diameter helical slow wave structures (grounded at the input end) mounted coaxially inside a 9.8 cm diameter outer cylindrical boundary is also plotted in Fig. 2. This data is for the case where the helix chirality (sense of helix winding) is such that the return current flowing in the helix produces an axial magnetic field in the same direction as that of the applied field. When the helix is wound with opposite chirality, much higher magnetic fields must be applied to achieve effective beam propagation. This result is consistent with the calculated transmission line impedance of about 600 ohms for the .07 pitch helix system and about 300 ohms average for the .1 + .27 pitch helix system, indicating that if the helices are charged up to a sizable fraction of the beam energy, the return current would be several kiloamperes, producing a large axial magnetic field, which may enhance or

*Work supported by the Air Force Office of Scientific Research and The Department of Energy.

0018-9499/83/0800-3183$01.00©1983 IEEE

detract from the applied magnetic field. The propagated current is virtually unchanged when the input end is floated, perhaps because inductive isolation after the first few turns allows effective charging of the helix even when the input end is grounded.

The arrival time of the peak electron beam current propagating in helix systems at the Faraday cup relative to that obtained in a cylindrical drift tube of the same diameter is plotted vs. applied magnetic field in Fig. 3. It is easily seen that substantial delays in the arrival time of the peak beam current are only observed for applied magnetic fields in the range 3-6 kilogauss, a result consistent with the expectation that both helix charging and beam-helix interaction should be maximized when the beam current flows near the helix wall.

An attempt to measure the beamfront velocity optically has been made using the configuration shown in Fig. 1. Plastic scintillant (NE102) was placed along the outside of the helix as shown, and light emitted when electrons struck the scintillant was picked up by fiber optic transmission lines. The light pipes were then aligned vertically in order of their axial position and the light observed was photographed using an image converter camera operating in the streak mode. Typical results obtained for both a fast and slow helix are shown in Fig. 4. These results show a beam front velocity of about 0.08 c for the .07 pitch helix and about .3 c for the .1 → .27 pitch helix. Both of these examples are for the case where the helix chirality was such that the return current in the helix produced a magnetic field that reduced the applied magnetic field behind the beam front. In this case, there is reason to believe that substantial beam current would strike the scintillant behind the beamfront. In the case where the helix field added to the applied field, the photographs are much more difficult to interpret, perhaps because electrons do not reach the scintillant as effectively.

III. Model of Solid Beam Equilibrium

To calculate the properties of an intense relativistic electron beam as a function of applied magnetic field and acceleration potential, we consider the system shown in Fig. 5. Our analysis assumes the beam expands adiabatically to a radius R_b where a laminar flow equilibrium is obtained far from the end walls. More specifically, a solid, uniform density electron beam of radius R_a is injected into a long, hollow, grounded drift tube of radius R_w. The entire system is immersed in a uniform axial magnetic field B_{AZ}. The injected beam is irrotational and monoenergetic with energy $mc^2(\gamma_o - 1) = eV_o$. The downstream beam properties shown in Fig. 5, ρ_b, V_ϕ, V_z, E_{sr}, $B_{s\phi}$, and B_{sz} along with the above assumptions are interrelated by:

Conservation of Particle Energy

$$\gamma(r) = \gamma_o + \frac{e}{mc^2}\phi(r) = \frac{1}{\sqrt{1 - \beta_\phi^2(r) - \beta_z^2(r)}}, \qquad (3)$$

where $\beta_\phi = V_\phi/c$, $\beta_z = V_z/c$, and $\phi(r)$ is the electric potential;

Conservation of Canonical Angular Momentum

$$-\frac{eB_{AZ}r_a^2}{2} = r\left[m\gamma(r)V_\phi(r) - eA_\phi(r)\right], \qquad (4)$$

where $A_\phi(r)$ is the downstream vector potential and r_a is the particles' radial position at the anode; and

Radial Force Balance

$$m\gamma(r)V_\phi^2(r)/r = e\{E_{sr}(r) + V_\phi(r)[B_{AZ} + B_{sz}(r)] - V_z(r)B_{s\phi}(r)\}. \qquad (5)$$

To solve the above equations, we assume the downstream charge density $\rho_b(r)$ is constant, i.e., $\rho_b(r) = \rho_b$, and $0 \le r \le R_b$. Then, the assumption of laminar flow implies the relative radial position of an electron in the beam is constant regardless of beam radius, i.e., $r/r_a = R_b/R_a$. Because E_{sr} is linear in r, we assume the azimuthal velocity is of the form $V_\phi = kr$. In addition, assuming $V_z(r)$ is relatively constant in r, $B_{s\phi}$ can be calculated by finding an $\bar{r}$ such that $V_z(\bar{r}) = \overline{V_z} \approx V_z(r)$. With the further assumption that all self magnetic fields are contained inside the conducting wall, we can calculate all self fields and potentials. Thus, knowing R_a, R_w, γ_o, and B_{AZ} and choosing the downstream beam radius R_b, we can then calculate the other equilibrium properties, ρ_b, $V_z(r)$, $V_\phi(r)$ via Eqs. (3)-(5). This procedure is iterated until the correct $\bar{r}$ is found. Finally, the total beam current is calculated by $I = \pi R_b^2 \rho_b V_z(\bar{r})$, which in steady state must equal the injected beam current.

Calculated beam properties are shown in Fig. 6 for the case $R_a = 1.0$ cm, $R_w = 4.8$ cm and $\gamma_o = 3.0$. These results show the variation of beam current with beam radius, externally applied magnetic field, and beam density. The beam density is expressed as the potential depression on axis divided by the acceleration voltage. We find that $\bar{r} = 0.5\ R_b$ gives the best fit. In the limit of B_{AZ} approaching infinity and when $\bar{r} = 0$, our results reduce to the Bogdankevich-Rukhadze curve with the limiting current given in Eq. (1) with f = 0. The calculations show our assumptions of $V_\phi(r)$ being linear in r and $V_z(r)$ being constant are quite good.

To interpret Fig. 6, select a magnetic field strength and follow that line until the injection current is reached, the beam radius equals the drift tube radius, or the beam becomes unstable. The current limit when the beam becomes unstable is due to loss of radial force balance occurring near the beam axis. On our curves, this region occurs at potential depths beyond the maximum current that can propagate for a given beam radius. If more current is injected than the system allows, the excess current is lost to the walls. For example, if $B_{AZ} = 1$ kG, 10.5 kA would propagate as a 3.6 cm beam, but a 20 kA injected beam would propagate as a 4.8 cm beam with only 17.25 kA. However, at $B_{AZ} = 1.5$ kG, a 4.8 cm beam will not propagate regardless of injection current; the largest beam at 1.5 kG is 3.6 cm at 12.5 kA current.

The above interpretation leads to Fig. 7 which compares theoretical predictions to experimental results. We have plotted maximum beam current vs. applied magnetic field for two wall radii, 4.8 cm and 1.9 cm. Experimental results, points "O" and "Δ," for these two cases are also displayed. When the applied magnetic field is relatively low, the beam current is limited, because the beam fills the tube. At higher magnetic field strengths, the beam current is limited by beam density, because electrons near the beam axis have large potential energies but insufficient kinetic energy to create the V×B forces which keep them in equilibrium. In this magnetic field regime, a virtual cathode forms if the injected current is above the steady state limit plotted. Though there is fairly good agreement between the solid beam model and the experimental data, we clearly need a less restrictive model.

References

1. C. N. Boyer, W. W. Destler, and H. Kim, IEEE Trans. Nucl. Sci. 24, 1625 (1977).
2. W. W. Destler, H. Kim, G. T. Zorn, and R. F. Hoeberling, in Collective Methods of Acceleration (N. Rostoker and M. Reiser, Eds.) Harwood Acad. Pub., 509 (1979).
3. L. S. Bogdankevich and A. A. Rukhadze, Sov. Phys. 14, 163 (1971).

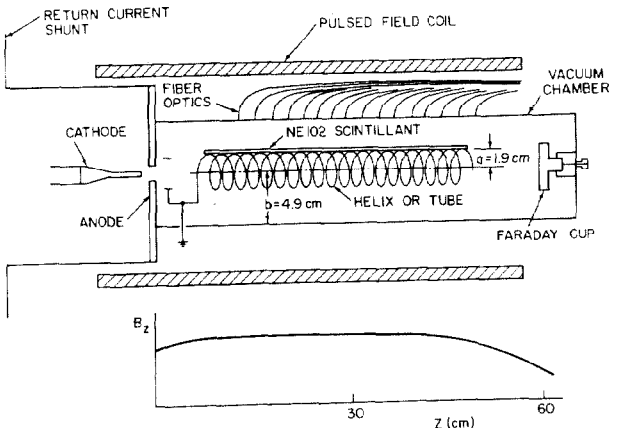

FIG. 1 General Experimental Configuration.

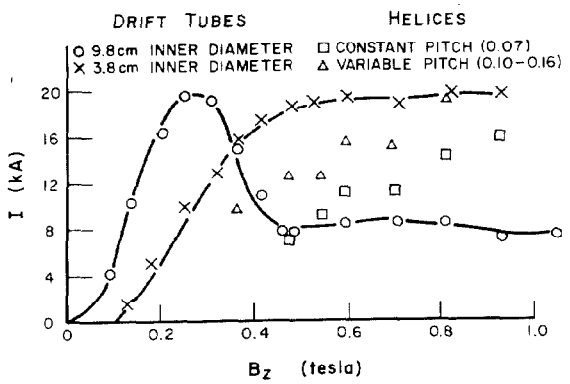

FIG. 2 Peak current propagated to the end of drift tube vs. applied magnetic field.

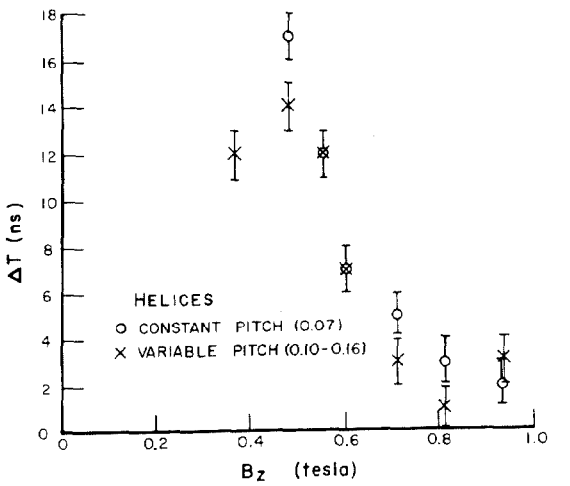

FIG. 3 Arrival time of peak current at Faraday cup vs. applied magnetic field relative to that obtained in a simple cylinder.

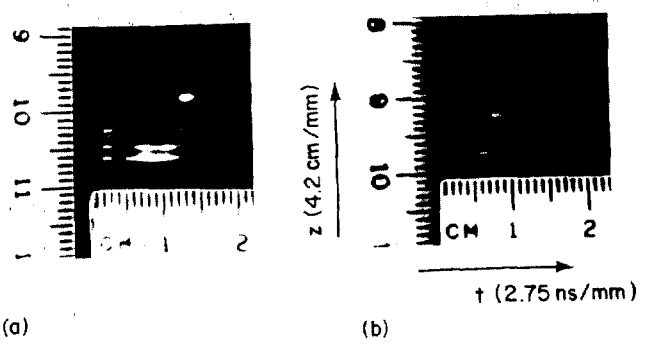

FIG. 4 Streak photographs of beamfront propagation velocity. a) .1 → .27 pitch helix, b) .07 pitch helix.

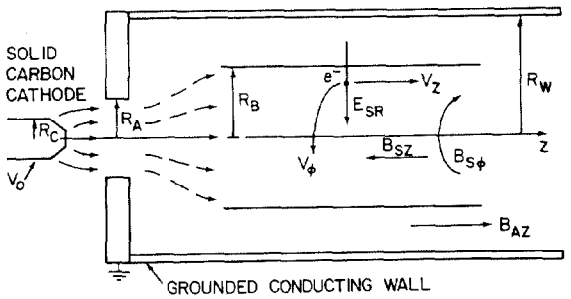

FIG. 5 Schematic of beam model.

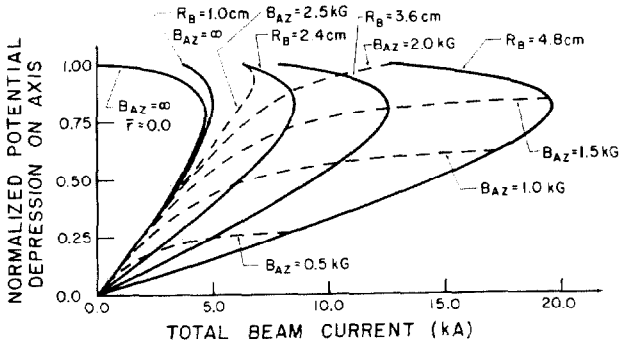

FIG. 6 Downstream beam properties for R_a = 1.0 cm, R_w = 4.8 cm, and γ_o = 3.0. Normalized potential depression on axis vs. axial current with beam radius R_b and applied magnetic field B_{AZ} as parameters.

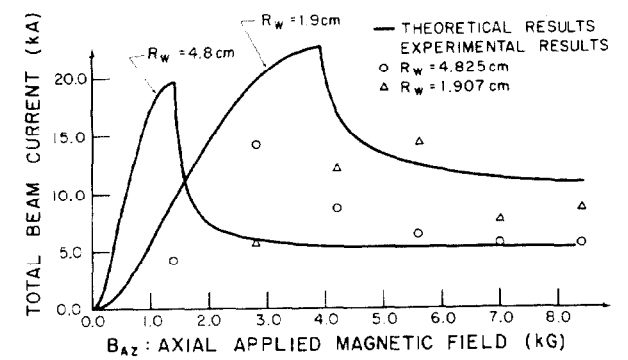

FIG. 7 Maximum beam current vs. applied magnetic field. Comparison of theoretical and experimental results for R_w = 4.8 and 1.9 cm.